NMR Solution Structure of the N3′ → P5′ Phosphoramidate Duplex d(CGCGAATTCGCG)$_2$ by the Iterative Relaxation Matrix Approach†

Daoyuan Ding,‡ Sergei M. Gryaznov,§ and W. David Wilson*,‡

Department of Chemistry, Georgia State University, Atlanta, Georgia 30303, and Lynx Therapeutics Inc., Hayward, California 94545

Received March 27, 1998; Revised Manuscript Received July 6, 1998

ABSTRACT: High-resolution 2D NMR spectra of the duplex CGCGAATTCGCG with deoxyribose sugars but with the normal phosphodiester linker replaced by an N3′ → P5′ phosphoramidate (NP) group have been used to establish a solution structure for the duplex. Distance, angle, and base pair hydrogen-bonding constraints were used to refine the structure by use of the iterative relaxation matrix approach (IRMA). The phosphoramidate NH proton signal could be observed in DMSO at low temperature but not in H_2O and D_2O. For this reason, the structure was refined with the −NH in each of the two possible low-energy configurations. The structure with the nitrogen lone pair located between the nonbridging oxygen atoms of the 5′-phosphate group consistently had the lowest energy and RMSD values, consistent with an X-ray analysis of the same duplex [Tereshko, V., Gryaznov, S., and Egli, M. (1998) *J. Am. Chem. Soc. 120*, 269−283]. In the refined structure, the sugars are in the C3′-endo conformation with the change from the normal C2′-endo conformation of deoxyribose apparently being driven by the gauche effect and the change in electronegativity from the 3′O to the 3′NH group. In agreement with preliminary studies [Ding, D., Gryaznov, S. M., Lloyd, D. H., Chandrasekaran, S., Yao, S., Ratmeyer, L., Pan, Y., and Wilson, W. D. (1996) *Nucleic Acids Res. 24*, 354−360], the backbone conformation in the NP duplex is very close to classical A-form values. Comparison of phosphodiester and phosphoramidate structures suggests that their backbones have global conformations that are primarily a function of the low-energy state of the sugar ring. A somewhat more complex situation arises when base pair conformation is analyzed with many of the base pairs having a conformation between those of classical A- and B-form helices. The effects of the 2′ substituent are obviously important in specifying the final conformation of the stacked bases in either an A-form or B-form helix. It is clear, however, that conversion of the normal phosphodiester of DNA into a phosphoramidate linkage yields a nucleic acid that behaves much more like RNA than DNA, and it has been shown that NP sequences can bind to RNA-directed proteins [Rigl, C. T., Lloyd, D. H., Tsou, D. S., Gryaznov, S. M., and Wilson, W. D. (1997) *Biochemistry 36*, 650−659].

Antisense therapeutic strategies have recently produced very promising results in clinical trials and are attracting considerable attention (*1*−*5*). The antisense method of drug development offers the promise of highly specific targeting and a resulting decrease in toxicity relative to other drugs that are generally available. The target of the antisense agents is a single-stranded section of a cellular RNA, typically a messenger RNA. Such RNAs have a structural preference for A-form helical regions with sugars in a C3′-endo conformation (*6*). First generation antisense oligonucleotides such as phosphorothioates and methylphosphonates, based on deoxyribose sugars, exist predominantly in C2′-endo conformations and prefer a B-form helix typical of DNA (*7*−*11*). These first generation agents generally form complexes with target RNAs that are less stable than similar complexes with unmodified DNA (*7*, *8*, *12*−*14*). Unmodified RNA of same sequence generally forms more stable duplexes with the target sequence than DNA. These results suggest that oligonucleotides which prefer an A-type conformation in the single-stranded state should provide pronounced enhancements of stability of duplexes with target RNAs, and they have sparked a search for second generation antisense agents with satisfactory nucleic acid modifications that prefer C3′-endo sugar geometries.

As part of the search for nuclease-stable linkages that form strong duplex complexes, phosphoramidate derivatives have been synthesized (*15*). Although the P3′ → N5′ phosphoramidate linkage yields unstable duplexes (*16*), oligonucleotides with the internucleoside N3′ → P5′ phosphoramidate linkage (Figure 1) form very stable duplexes and triplexes with complementary nucleic acid phosphodiester and phosphoramidate strands (*17*−*21*). Since the N3′ → P5′ phosphoramidate (NP) monoester internucleoside linkage is not chiral, is nuclease resistant, and has the same formal charge as phosphodiesters, it provides a very attractive backbone for development of antisense therapeutics. Initial tests of a phosphoramidate oligomer as an antisense agent have produced very favorable results (*17*). Preliminary NMR

† This work was supported by NIH Grant GM-54896. The NMR instruments were purchased through funds from the NSF (STI 9214443) and the Georgia Research Alliance.

* To whom correspondence should be addressed.

‡ Georgia State University.

§ Lynx Therapeutics Inc. Present address: Geron Corp., 230 Constitution Drive, Menlo Park, CA 94025.

S0006-2960(98)00711-9 CCC: $15.00
Published on Web 08/13/1998

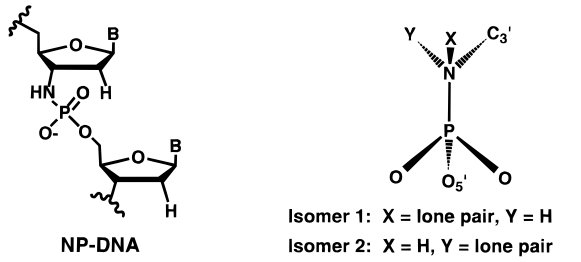

FIGURE 1: Structure (left) of the N3′ → P5′ phosphoramidate-modified backbone and the two low-energy configurations (right) of the N3′ → P5′ group. Isomer 1: X = lone pair, Y = H. Isomer 2: X = H, Y = lone pair. The ζ angle (C3′−N−P−O5′) of the nucleic acid backbone is g^- in the diagram as usually observed in nucleic acid duplexes. In natural DNA and RNA, the NH is replaced by O3′.

studies and CD experiments have suggested that duplexes from NP strands adopt an A-form helical conformation (*18*). Since the NP backbone is based on deoxyribose sugars, this is a surprising finding since no mixed-sequence deoxyribose phosphate based duplex has an A-form structure under standard solvent and temperature conditions. In addition to the NMR and CD results, an A-form structure for the phosphoramidate duplex is also supported by recent X-ray crystallographic (*22*) and unrestrained molecular dynamics (*23*) results. The A-form structure offers an explanation for at least part of the enhancement in stability of NP·RNA heteroduplexes in antisense applications.

The finding of a nuclease-stable A-form nucleic acid strand with low toxicity has also suggested the possibility of preparation of RNA exogenous decoys as antiviral agents (*21*). Regulation of replication in HIV-1, for example, requires binding of two trans-acting proteins, Rev and Tat, to two respective cis-acting RNA binding sites, RRE and TAR (reviewed in refs *24*−*27*). These regulatory proteins provide tight control over HIV-1 replication and efficient use of the limited nucleotide sequences in the viral genome. The key roles of these viral proteins make them attractive targets for drug intervention, but there are as yet no good clinical candidates that target Rev or Tat. Endogenous therapeutic RNA or decoys, produced in vivo through genetic manipulation, have been successfully designed to mimic the structure of the RRE or TAR duplex structures that bind Rev or Tat (*28*, *29*). This mimicry enables the decoy to compete with the natural RNA as it attempts to interact with specific proteins within the cell. Conversion of this approach to exogenous RNA decoys offers an attractive strategy for antiviral drug development, and initial results suggest that the method can be successfully applied to the RRE-Rev and TAR-TAT complexes of HIV-1 (*21*).

The structural basis for these exciting applications of N3′ → P5′ phosphoramidate duplexes is not yet fully developed, and it is essential to obtain a detailed solution structure of a phosphoramidate duplex to evaluate its relationship to classical A- and B-form helical structures, the region of RNA binding proteins that could be targeted with NP decoys, and the molecular basis for the helical structure of this deoxyribose-based backbone. The sequence CGCGAAT(U)T(U)CGCG has been analyzed in detail by X-ray and NMR methods as both DNA (*30*, *31*) and RNA (*32*). The DNA sequence forms a B-type helix while the RNA is an A-form. We report here the solution structure of an NP duplex of sequence CGCGAATTCGCG and compare the structures to literature results for the same sequence as phosphodiester DNA (*30*, *31*) and RNA (*32*), as well as to results of solid state (*22*) and modeling analysis (*23*) on the NP backbone.

MATERIALS AND METHODS

Samples. The N3′ → P5′ phosphoramidate dodecamer duplex np$(CGCGAATTCGCG)_2$ and dinucleoside dTnpT were synthesized, purified, and characterized as previously described (*18*). The sample was dissolved in 0.6 mL of 99.96% D_2O, lyophilized several times, and finally dissolved in 99.996% D_2O for NMR experiments. Exchangeable proton spectra were obtained in 90% H_2O/10% D_2O (v/v). Spectra for the dodecamer were collected in an ∼1 mM (per duplex) solution containing 7.5 mM phosphate, 0.01 mM EDTA, 100 mM NaCl, pH 7.0. Proton NMR spectra for the dinucleoside TnpT with a linking phosphoramidate group and terminal deoxyribose were obtained in DMSO and in D_2O. Experiments were done at 25 °C unless otherwise indicated.

NMR Experiments. All NMR spectra were acquired with a Varian Unity Plus 600 MHz spectrometer. The NMR data were processed with Vnmr or were transferred to a Silicon Graphics workstation and processed with Felix 95.0 software. 1D spectra were collected with a spectral width of 5000 Hz and 32K data points. The 1D exchangeable proton spectrum in H_2O was collected with the Binom pulse sequence (*33*) at 2 °C.

NOESY spectra in 99.996% D_2O at six mixing times (50, 75, 100, 150, 200, 300 ms) were recorded with spectral widths of 5100 Hz in both dimensions, 2048 complex points in the acquisition dimension, and 256 t_1 increments. For each increment, 24 scans were collected with a relaxation delay of 5 s. Data were zero-filled to 2K points in both dimensions. NOESY spectra at 0 °C in 90% H_2O/10% D_2O with mixing times of 100, 200, and 300 ms were collected with the WATERGATE pulse sequence (*34*) over spectral widths of 14 000 Hz in D_1 and 7198 Hz in D_2 and 4096 t_2 complex points with 112 t_1 increments, each the average of 112 transients. The number of t_1 increments in 2D experiments was selected to optimize the S/N ratio with acceptable resolution. After zero-filling a data set of 4K × 4K was obtained.

TOCSY experiments (40 and 120 ms isotropic mixing times) were recorded with spectral widths of 5800 Hz in both dimensions with 56 scans per t_1 increments and data sizes of 2048 points in t_2 and 256 in t_1. Data were zero-filled to 2K × 2K. The DQF-COSY was collected with 4096 data points in t_2 and 256 data points in t_1, and data were zero-filled to 4K × 1K. All of 2D NMR data were acquired in the phase-sensitive mode using the State−Haberkorn method and were apodized with a sine-bell function shifted by 90°.

To assign the phosphorus resonances, a nonselective proton-detected $^1H-^{31}P$ heteronuclear correlation experiment (*35*) was carried out with 2048 complex points over a spectral width of 1120 Hz in the proton dimension and 512 data points over a spectral width of 1480 Hz in the phosphorus dimension. A selective $^1H-^{31}P$ heteronuclear correlation experiment using an IBURP-shaped pulse (*36*) was used to determine H3′−P coupling constants. The data were ac-

quired using the States−TPPI method of phase cycling and were apodized with a sine-bell function shifted by 90°.

Restraint Generation. Initial NOE distance restraints involving nonexchangeable protons were obtained from the cross-peak volumes in 2D NOESY spectra at all mixing times. The volumes of 204 clearly resolved NOESY cross peaks were obtained by directed integration using the "box method" in the Felix software. Distances were calculated from the volumes with the cytidine H5−H6 (2.48 Å) cross peak as reference (*37*). The initial NOE distance restraints were derived from NOE buildup rates. Initial buildup rates were obtained by fitting the NOE volumes as a function of mixing times to a second-order polynomial. The initial bounds were set to ±30%. For the overlapped cross peaks, the total volume was determined and individual peak volumes were approximated by dividing the total volume by the number of cross peaks that overlapped. The distance bounds of 52 overlapped cross peaks were estimated on the basis of these volumes. Because of the approximation involved, the bounds for these distance restraints were set to 30% and were kept constant during structure calculations.

A total of 27 NOEs involving exchangeable proton resonances were classified as strong (cross peaks appear in 100 ms NOESY spectrum), medium (appear in 200 ms but not 100 ms spectrum), or weak (only appear in 300 ms spectrum) on the basis of visual inspection of intensities from NOESY spectra at 100, 200, and 300 ms and corresponding to 2−3.5, 2−4.5, and 2−6 Å distance-bound ranges. A total of 32 Watson−Crick hydrogen-bonding restraints on the 12 base pairs were included based on 1D and 2D imino peaks in H_2O. Restraint ranges are on the basis of base-pair structural information (*6*). Torsion angle restraints were obtained from coupling constant analysis as described below.

Structure Calculations. Structure calculations were performed on a Silicon Graphics computer using the NMRchitect and DISCOVER (Version 2.9) modules within the MSI software package. Calculations employed the AMBER force field in a vacuum, excluding counterions and solvent molecules. The charges around phosphate groups were reduced as previously described to more accurately mimic the solvent and charge environment of the nucleic acid backbone (*38*). The bond lengths and bond angles of the phosphoramidate group were determined initially from ab initio calculations (*39*) and later from a crystal structure (*22*) of the same NP duplex when the crystal structure became available. Nonbonding terms included van der Waals energies with a Lennard-Jones function and an atom pair distance cutoff of 12 Å. A distance-dependent dielectric constant of 4*r* was used in calculation of the electrostatic energy term. The energy terms for distance and torsion angle restraints are calculated with flat-bottomed quadratic potentials.

The iterative relaxation matrix approach (IRMA) (*40*) was used to generate more accurate distance restraints using methods similar to those recently described for RNA (*41*) and DNA (*42*) structures. During the IRMA process, the 204 distance restraints from well-resolved cross peaks were refined, and differences between the experimental NOE and back-calculated NOE intensities serve as criteria for convergence of the structure. As part of each IRMA cycle, a protocol including restrained molecular dynamics (rMD) and restrained energy minimization (rEM) was executed to minimize the structure based on the 204 refined distance restraints per duplex, as well as 90 torsion angle restraints, 27 exchangeable proton distance restraints, 32 hydrogen-bonding distance restraints, and 52 nonexchangeable proton distance restraints from partially overlapped cross peaks.

Different initial structures and structure refinement protocols were used to ensure that the same final structure was obtained on approach from different starting directions. In the first protocol two starting structures were built with the InsightII software package from classical A- and B-form coordinates for the np$(CGCGAATTCGCG)_2$ duplex with the N3′ → P5′ modified backbone. Because there could be two isomers at the phosphoramidate group (Figure 1), based on the different orientations along which hydrogen is attached to the backbone nitrogen, four initial structures have been generated: A-form isomer 1, A-form isomer 2, B-form isomer 1, and B-form isomer 2. The four initial structures were subjected to rMD and rEM: (a) 2000 cycles of conjugate gradient rEM, (b) 100 ps of rMD at 300K with a step size of 1 fs, (c) 500 iterations of steepest rEM, and (d) 2000 iterations of conjugate gradient rEM. The restraints were kept throughout the calculation. The multiplication factors for force constants of covalent and restraint terms were set to full scale, and 1−4 nonbonding terms were set to 0.5. The force constants for NOE and torsion angle restraints were set to 20 kcal/(mol·Å^2) and 30 kcal/(mol·rad^2), respectively. This protocol was combined with RMA. This process was repeated until the best match between experimental NOESY and theoretical NOESY spectra back-calculated from the refined structure was obtained. Four final structures were obtained after final energy minimization in this protocol, two from isomer 1 and two from isomer 2.

To more widely sample conformational space, a second protocol with high-temperature simulated annealing was used. In this protocol two average structures, one from averaging of the two final structures of isomer 1 and another from averaging of two final structures of isomer 2, were used as the starting structures. The procedure was (a) 500 cycles of steepest decent rEM without nonbonding, electrostatic, and torsion angle restraints terms and with small distance restraint terms; (b) 12 ps of rMD at 1000 K with small distance restraint terms (multiplication factor 0.3), very small torsion angle (0.01) and nonbonding (0.05) terms, and no electrostatic terms; (c) 8 ps of rMD with temperature gradually decreased from 1000 to 300 K and nonbonding terms increasing from 0.05 to 0.40, distance restraint terms increasing from 0.3 to 1.0, torsion angle restraint terms increasing from 0.1 to 0.8, and no electrostatic term; (d) 3 ps of rMD at 300 K with full value restraint terms, the 1−4 nonbonding term at 0.5, and no electrostatic term; (e) 500 iterations of steepest decent rEM with full scale values for nonbonding and restraint terms; (f) 3 ps of rMD at 300 K to prevent the molecule from being trapped in a local energy minimum; (g) 500 iterations of steepest decent rEM; and (h) 2000 iterations of conjugate gradient rEM. Thirty-two structures were generated during step b of the simulating annealing protocol, 16 from isomer 1 and 16 from isomer 2; they were then refined by combining IRMA with the above protocol. The structures were analyzed through inspection of their geometries, *R*-factors, energies, and restraint violations. Five structures from isomer 1, and five from isomer 2, with reasonable geometries, lower *R*-factors, energies, and

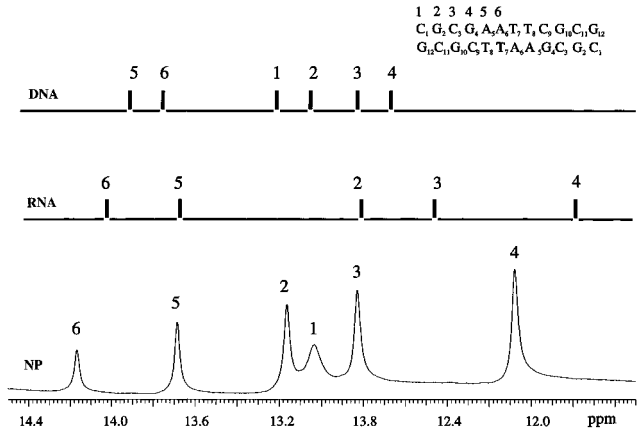

FIGURE 2: One-dimensional proton NMR spectrum in the imino region of N3′ → P5′ phosphoramidate CGCGAATTCGCG in 90% H_2O/10% D_2O at 2 °C. The assignments for unmodified DNA (*31*) and RNA (*32*) with same sequence are shown for comparison.

smaller restraint violations were selected, and the final structures for isomer 1 and isomer 2 were obtained by minimizing the average structures.

During the IRMA calculations, a series of *R*-factors were derived in each cycle, representing differences between experimental and theoretical NOE intensities. The most important *R*-factors are defined as $R_1 = \sum|A^{theo} - A^{expt}|/\sum A^{expt}$, $R_2 = \sum t_m|A^{theo} - A^{expt}|/\sum t_m A^{expt}$, $R_7 = \sum|A^{theo} - A^{expt}|/\sum 0.5(|A^{theo} + A^{expt}|)$, and $R_8 = \sum t_m|A^{theo} - A^{expt}|/\sum t_m 0.5(|A^{theo}| + |A^{expt}|)$, where A^{expt} and A^{theo} are the NOE intensities of experimental and theoretical NOE matrixes and t_m is the mixing time. The iterative process was repeated until the *R*-factors did not change significantly. The final structures were used to back-calculate the theoretical NOESY spectra using the Model module in Felix 95.0 with a mixing time of 0.3 s and an isotropic correlation time of 3 s. The correlation time was determined by fitting the NOEs of the cytosine H5−H6 proton pairs over a series of mixing times (*43*).

RESULTS

Resonance Assignments. Nonexchangeable proton signals for np(CGCGAATTCGCG)$_2$ have been previously assigned (*18*). A 1D spectrum in the imino region is shown in Figure 2 along with published assignments for DNA (*31*) and RNA (*32*) of corresponding sequence for comparison. Exchangeable proton signals for the imino and observable amino protons were assigned from 2D NOESY spectra obtained in 90% H_2O/10% D_2O (v/v) (Figure S1, Supporting Information) and are listed in Table 1. Phosphoramidate NH resonances were not observed under these conditions.

To investigate the phosphoramidate NH signals, proton NMR spectra of TnpT in DMSO were obtained and revealed three exchangeable upfield resonances (5.4, 6.2, and 6.6 ppm) as well as the downfield imino proton signals that are not observed in D_2O. The peak at 6.2 ppm is much broader than the other exchangeable signals at 25 °C but becomes much sharper as the temperature is decreased. A DQF-COSY spectrum at 15 °C revealed a cross peak between the H3′ proton of the Tnp nucleotide and the 6.2 ppm signal, thus assigning the 6.2 ppm resonance to the phosphoramidate NH proton. The signals at 6.6 and 5.4 ppm were assigned to the 5′ and 3′ hydroxyl protons, respectively, on the basis of NOESY spectra and analogy with phosphodiester dinucleosides. A 1D proton NMR spectrum along with a 1D NOESY slice along the water resonance in the DMSO solvent is shown in Figure 3. The peaks in Figure 3B are in-phase with water, indicating a very fast exchange rate for the NH proton with water, and this observation explains why the NH protons are not observed in H_2O solutions of TnpT or in the dodecamer duplex spectra.

Phosphorus signals for np(CGCGAATTCGCG)$_2$ were assigned from nonselective (*35*) and selective (*36*) proton-detected $^1H-^{31}P$ heteronuclear correlation experiments through connections to 3′ protons (Figure S2, Supporting Information and Table 1). Four ^{31}P signals overlap at approximately 1.3 ppm (Table 1). Relative to phosphodiester DNA, there are large downfield shifts (∼5 ppm) for NP phosphorus signals and large upfield shifts for the H3′ proton signals. The difference in H3′ chemical shifts can be seen directly by comparing the H3′ chemical shift for G12 (with a 3′-OH) in Table 1 to the H3′ chemical shifts for all other residues in the duplex. Although chemical shifts depend on several factors, the significant upfield shift of the H3′ signals on substitution of the 3′O for a 3′NH is expected for the switch from the more electronegative oxygen to the NH group. $^1H-^{31}P$ coupling constants were extracted from a selective $^1H-^{31}P$ heteronuclear correlation experiment (Figure S2, Supporting Information) and are also given in Table 1.

Force Field Modifications. New parameters for the phosphoramidate group must be added to the AMBER force field (*44*) for rMD and rEM calculations involving the NP group. Calculations were done with optimum bond lengths and angles determined from ab initio calculations (*39*) and from an X-ray structure of the np(CGCGAATTCGCG)$_2$ duplex (*22*). Very similar final structures were obtained with the two parameter sets. The stretch, bend, and torsion force constants were assigned to the NP group by analogy with the phosphate constants in AMBER (*44*). The bond stretch force constants for the NQ-P and CT-NQ bonds (Table 2) were set slightly higher than in the unmodified backbone in order to model the possible conjugation in the NP group (*22*). The angle bending force constants are taken from the AMBER values for the phosphodiester group (Table 2). The torsion force constants for X−NQ−P−X and X−CT−NQ-X bonds were set to $V_{3/2} = 0.5$ with $n = 3$.

NMR-Based Structural Constraints. Torsion Angles. Torsion angle restraints for the β backbone angles can be derived from P−H5′/H5″ coupling constants (*45*). Since all cross-peak intensities from P−H5′,H5" are very weak in $^1H-^{31}P$ heteronuclear correlation spectra (Figure S2, Supporting Information), β angles must be trans for nucleotides G2 to G12 (*45*). A gauche$^+$ or gauche$^-$ β angle would result in a significantly larger coupling constant for either P−H5′ or P−H5″ in the heteronuclear experiment in contrast to what is observed. All β angles were restrained to 180 ± 30°, which is the range of both classical A-form and B-form structures, in the rMD calculations. The γ backbone angles can be derived from H4′−H5′ and H4′−H5" couplings (*45*). Unfortunately, the cross peaks in this region from the DQF-COSY spectra were heavily overlapped, and it is impossible to get precise H4′−H5′,H5" coupling information. The TOCSY spectra at different mixing times (40 and 120 ms) reveal that there are cross peaks from H3′−H4′ but not from H3′−H5′,H5" in all nucleotides (see Figure S3, Supporting Information). The H4′−H5′,H5" couplings must then be

Table 1: Assignment (in ppm) of Proton and Phosphorus Signals and Phosphorus−H3′ Proton Coupling Constants (in Hz, ±2) of the Phosphoramidate-Modified d(CGCGAATTCGCG)$_2$[a]

	H6/H8	H1′	H2′	H2″	H3′	H4′	H5′/H5″	H5/CH3	H2	imino	amino	^{31}P	$J_{P-H3'}$
C1	8.19	5.80	2.70	2.34	3.68	3.93	4.03/4.07	6.03					
G2	7.98	5.99	2.70	2.40	3.86	4.04	4.13/4.24			13.13		∼1.3	
C3	7.85	5.71	2.74	2.30	3.69	4.00	4.10/4.23	5.34			6.67/8.42	1.14	12.5
G4	7.64	5.90	2.70	2.40	3.73	4.03				12.03		∼1.3	
A5	7.90	6.10	2.89	2.42	3.79	4.08	4.10/4.25		7.16		6.57/7.88	∼1.3	
A6	7.64	6.01	2.71	2.46	3.56	4.08			7.72		6.85/8.15	1.28	12.5
T7	7.59	5.67	2.55	2.32	3.62	4.02	4.06/4.22	1.18		14.12		0.59	13.1
T8	8.10	5.84	2.59	2.32	3.80	4.00	4.11/4.23	1.56		13.62		0.85	14.7
C9	8.02	5.69	2.59	2.31	3.70	3.97	4.09/4.23	5.62			6.62/8.35	1.47	13.0
G10	7.77	5.84	2.58	2.30	3.73	3.98	4.07/4.18			12.77		1.67	12.6
C11	7.78	5.70	2.58	2.43	3.70	4.00		5.26			6.80/8.50	0.99	14.0
G12	7.78	6.18	2.32	2.42	4.54	4.12				12.98		∼1.3	

[a] Nonexchangeable proton assignments were from ref *18*. Imino and amino protons were assigned on the basis of 1D Binom and 2D NOESY watergate experiments at 2 °C. ^{31}P chemical shifts were assigned on the basis of the H−P HETCOR experiment at 25 °C and referenced to TMP. P−H3′ coupling constants were extracted from a selective H−P HETCOR experiment at 25 °C.

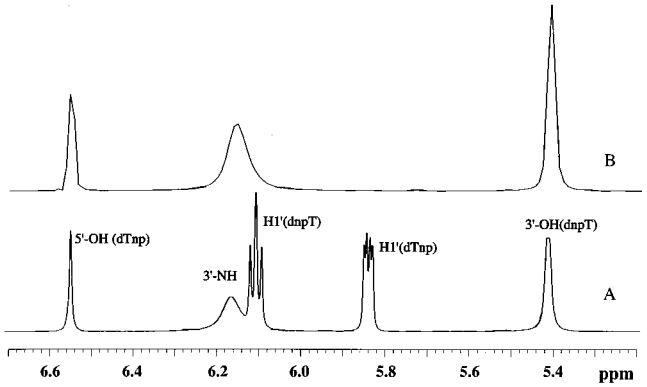

FIGURE 3: (A) One-dimensional proton NMR spectrum of dTnpT in DMSO at 15 °C. (B) One-dimensional NOESY slice along the water resonance. The NOESY spectrum was obtained with a mixing time of 300 ms in DMSO at 15 °C.

Table 2: Nonstandard Force Field Parameters for the Phosphoramidate Backbone in the Calculations[a]

	bond parameters	
	K_r [kcal/(mol·Å^2)]	bond length (Å)
NQ−P	367	1.609
CT−NQ	367	1.437
H−NQ	434	0.998
P−OS	230	1.591
	angle parameters	
	K_o [kcal/(mol·rad^2)]	angle value (deg)
CT−CT−NQ	80	111.91
CT−CT−NQ	80	111.91
CT−NQ−P	100	120.33
NQ−P−O2	100	108.34
NQ−P−Os	100	104.67
	dihedral parameters	
	V_n (kcal/mol)	r (deg)	n
−NQ−P−	0.5	0	3
−CT−NQ−	0.5	0	3

[a] Atom type of nitrogen in phosphoramidate linkage is NQ.

weak in order to prevent coherence transfer from H3′ to H5′,-H5". In this case the predominant conformation for γ must be gauche$^+$ and all γ angles were loosely restrained to 60 ± 40°, as in classical A- and B-form conformations. The δ torsion angles are extremely important for specifying the deoxyribose conformation and were determined on the basis of deoxyribose coupling patterns in DQF-COSY (*18*) spectra. The fact that there are no cross peaks for H1′−H2′ in the nucleotides from C1 to C11 strongly indicates that the sugar

Table 3: Number and Type of Distance and Torsion Angle Restraints Used in the Structure Calculation

distance				315
	NOE	nonexchangeable[a]	intraresidue	140
			interresidue	112
			interstrand	4
		exchangeable	intra base pair	14
			intra base pair	13
	hydrogen bonding			32
torsion angle				90

[a] 204 restraints from well-isolated NOE cross peaks were refined during IRMA calculation. 52 from overlapped NOE cross peaks were used as distance restraints that were kept constant in the calculation.

conformations are C3′-endo, and δ angles for C1 to C11 residues were restrained to 80 ± 15°, the C3′-endo value. The torsion angles α and ζ are related to the phosphorus chemical shift values in unmodified DNA (*45*). A small range of chemical shifts (about 1 ppm or less) centered at −4.4 ppm has been used to exclude the trans conformation. In the DNA with phosphoramidate modifications, the phosphorus resonances are centered at approximately 1 ppm within a chemical shift range of only 1.1 ppm (Table 1), suggesting a tight range of α and ζ angles in the normal A- and B-form conformational range. The α angles, which are not directly involved in bonding to the NP nitrogen of the modified backbone, can, thus, be restrained to ±120° which covers both A and B conformations. Since the ζ angle involves direct bonding of the phosphoramidate N, it was not restrained. The torsion angle ϵ in unmodified DNA can been derived from H3′(n) − P(n+ 1) J-couplings (Table 1), but the ϵ angles were not restrained here because we do not yet have Karplus parameters for the NP group.

NMR-Based Structural Constraints. Interproton Distances. Proton−proton distance restraints were generated as described in Materials and Methods, and all constraints used in the structure calculations are listed in Table 3. No planarity constraints were introduced in the refinement.

Structure Calculations. As described in Materials and Methods, different structure calculation protocols were used with different starting structures to ensure that the same final structure was approached from different regions of conformational space. In first structure calculation protocol, four initial structures, two from the classical A-form with isomer 1 and isomer 2 and two from the classical B-form DNA with

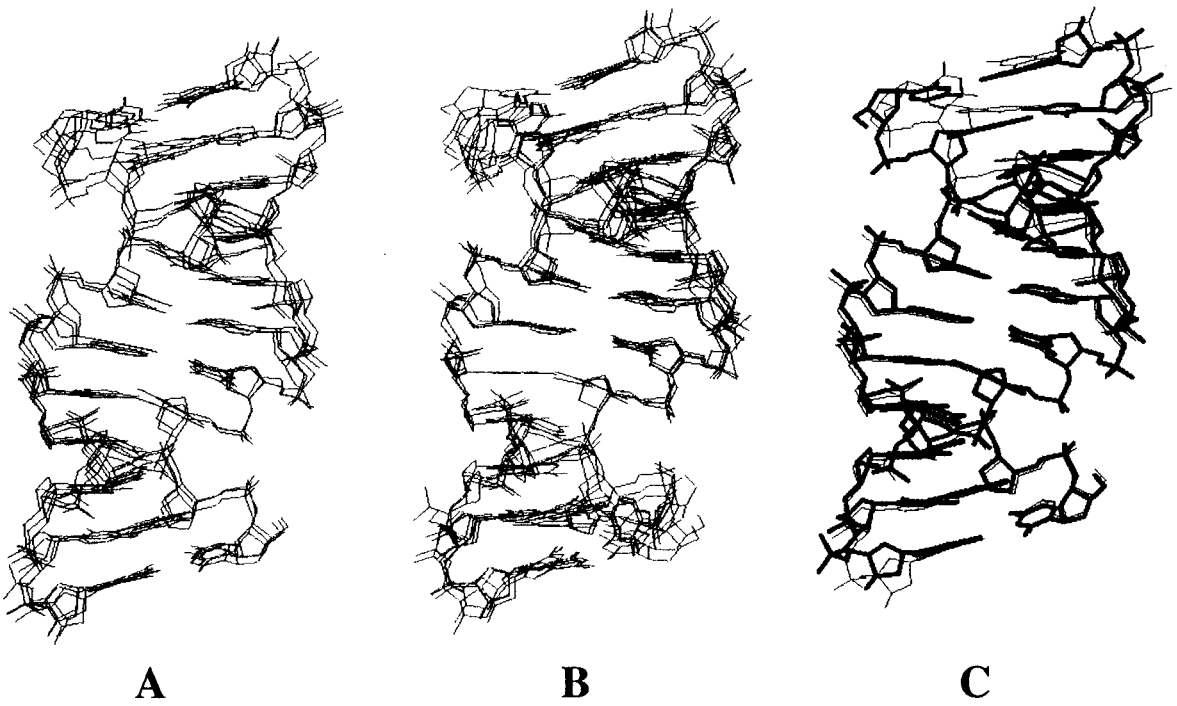

FIGURE 4: Superpositions of the five best calculated structures of N3′ → P5′ phosphoramidate DNA from isomer 1 (A) and isomer 2 (B). Energy-minimized final structures from both isomers are shown superimposed in (C).

both NP isomers, were generated in InsightII. The four structures were submitted to rMD and rEM with IRMA for refinement. Over the course of five IRMA iterations, convergence was indicated by the leveling off of *R*-factors. The two resulting structures from isomer 1 overlapped with a heavy atom pairwise RMSD of 0.77, while the two structures from isomer 2 overlapped with a RMSD of 0.85. In a second protocol, two average structures, one from averaging of two structures of isomer 1 and another from averaging two structures of isomer 2, were submitted to high-temperature simulated annealing (SA) in order to search wide regions of conformational space. Structure refinement was done with rMD, IRMA, and final rEM (see Materials and Methods). Structures for refinement were periodically selected from the ensemble generated during 12 ps of molecular dynamics with very small restraints at 1000 K, 16 structures from isomer 1 and 16 from isomer 2. Because of the high temperature and small restraints used, the 32 structures provide very different starting conformations for refinement, and they were submitted to the next cycle separately. Five iterations through the refinement protocol resulted in leveling off of *R*-factors.

Based on analysis of their geometries, *R*-factors, energies, and restraint violations, five optimum structures from isomer 1, which overlapped with a average heavy atom RMSD of 0.46, and five from isomer 2, which overlapped with a average heavy atom RMSD of 0.65, were selected. Figure 4 shows the superpositions of five structures from isomer 1 (Figure 4A) and five structures from isomer 2 (Figure 4B) and indicates that the same conformation is approached from very different regions of conformational space. The five structures from isomer 1 and, separately, the five from isomer 2 were averaged to give two ensemble averages. Energy minimization calculations were then performed on the two-ensemble average of structures to give a single final structure for isomer 1 and another for isomer 2. The energy for the isomer 1 structure is significantly lower than for the isomer 2 structure after rEM (−234.8 kcal/mol from isomer 1 vs −214.6 kcal/mol from isomer 2). The two energy-minimized final structures are shown superimposed in Figure 4C. The overlap of the two structures is excellent for the central 10 base pairs, but there is more variation in the terminal base pairs. An additional comparison is provided in Figure 6 where the energy-minimized isomer 1 structure is compared to structures for classical A and B duplexes of the same sequence as well as to the Egli crystal structure (*22*) of the NP duplex.

Structure Analysis. The nucleotide chirality was checked using the method of Schultze and Feigon (*46*), and no chirality changes occurred during the calculations. Figure 5 shows a plot of restrained distances versus actual distances for the final isomer 1 and 2 structures. The great majority of distances and all distances with the largest NOE values satisfy the restraints within ±20%. There are no torsional angle violations for either final structure within the bounds that were used in the structure calculations described above.

A more rigorous test of structural accuracy is back-calculation of NOESY spectra from the final structures and comparison of calculated and experimental NOESY spectra. Figure 7 shows comparisons of representative regions of experimental and back-calculated 300 ms NOESY spectra from final isomers 1 and 2. The excellent match between experimental and back-calculated spectra indicates that the final structures not only satisfy the proton−proton distance restraints but also are consistent with the entire proton relaxation network that generates the time-dependent NOESY spectra. The back-calculated spectra for both isomer 1 and isomer 2 match the experimental results quite closely, and in all spectral regions, the experimental and back-calculated spectra are in excellent agreement. The back-calculated spectra for classical B-form and A-form structures as well

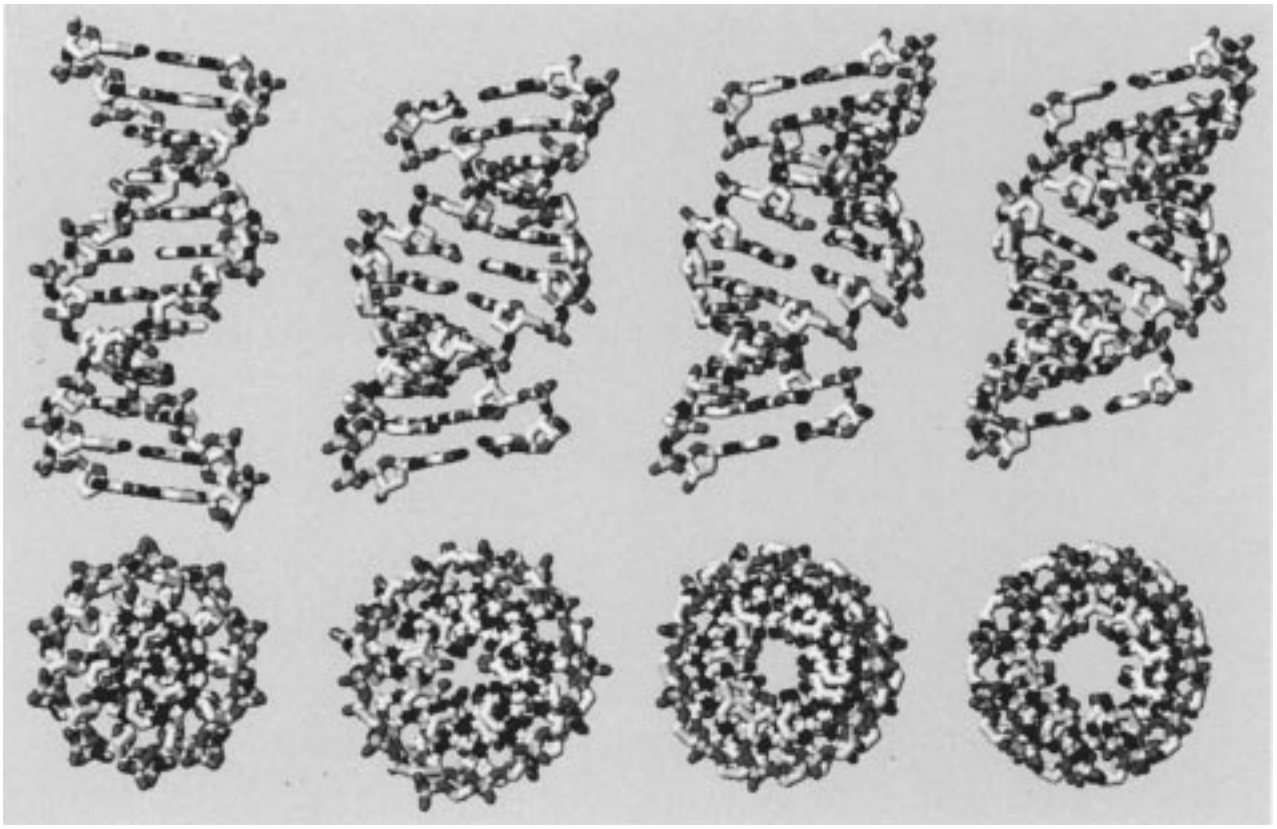

FIGURE 5: Final structure for isomer 1 (second to left, from Figure 4C), the NP crystal structure (*22*, third to left), and classical A-form (right-most) and classical B-form (left-most) structures built in InsightII.

as for the crystal structure (*22*) of the same sequence are also shown in Figure 7 for reference. It is clear that both classic B-form and A-form duplex structures yield NOESY plots that differ significantly from the experimental spectrum and that the B-form duplex is the most different from the experimental structure. Although the final structure is much closer to the A-form than to the B-form helix, there are several spectral regions where the experimental and back-calculated spectra from the A-form have different numbers of cross peaks, as well as cross peaks with obvious differences in intensity.

Back-calculated NOESY spectra (Figure 7) for the crystal structure are also in good agreement with the experimental 2D plots and are much closer to the experimental spectra than to those for either the classical A-form or B-form spectra. In the aromatic to H2′/H2" cross-peak region, which is a good monitor of similarity of backbone geometry, the experimental and crystal NOESY plots are in excellent agreement. In the aromatic to H1′ region, which is a good monitor of helix characteristics, as well as backbone geometry, all but one of the experimental cross peaks are represented in the NOESY plot for the crystal structure. The T8H1′ → C9H6 (5.84 → 8.02 ppm) cross peak is missing in the crystal spectrum, and several cross peaks, such as the A5H2 → C9H1′ (7.16 → 5.69 ppm) that monitor helix parameters, minor groove topology in this case, differ significantly in intensity between the experimental and crystal NOESY plots. The results of these small differences can also be observed as slight structural differences between the solution and X-ray models (Figure 5).

Another test for the quality of the final structures is based on the four *R*-factors described in Materials and Methods, which were calculated for all well-resolved cross peaks from the NOESY spectra (Table 4). The *R* values of the final structures, independent of the calculation protocols, are the lowest, indicating overall good agreement between the final structures and NMR data. The backbone, glycosidic torsion angles (Table S1, Supporting Information) and helical parameters of final structures were analyzed using the NEWHEL93 program of R. E. Dickerson. The helical parameters base pair inclination, *x*-displacement, rise, and twist have characteristic values for the A- and B-helical structures, and these values are plotted in Figure 8 for the final isomer 1 and isomer 2 structures shown in Figure 4C. Values for the same helical parameters are also plotted in Figure 8 for the classical A- and B-helical forms as well as for crystal structures of the phosphodiester (*30*) and phosphoramidate (*22*) dodecamer duplexes for comparison.

DISCUSSION

Oligomers with N3′ → P5′ phosphoramidate linkages have shown extremely promising properties as "second generation" antisense therapeutic agents, as potential antigene agents through their ability to form very stable triplexes with DNA duplexes, and as decoys for RNA-binding proteins (*15*−*23*). In an effort to better understand the structural basis and interaction principles responsible for the favorable properties of the phosphoramidates, several structural studies have been carried out. We have reported a preliminary NMR and CD analysis of the self-complementary NP duplex, np(CGCGAATTCGCG)$_2$ (*18*), and the same duplex has been studied by molecular dynamics methods (*23*) and by X-ray crystallography (*22*). Our high-resolution solution structure reported here agrees with the preliminary NMR results and

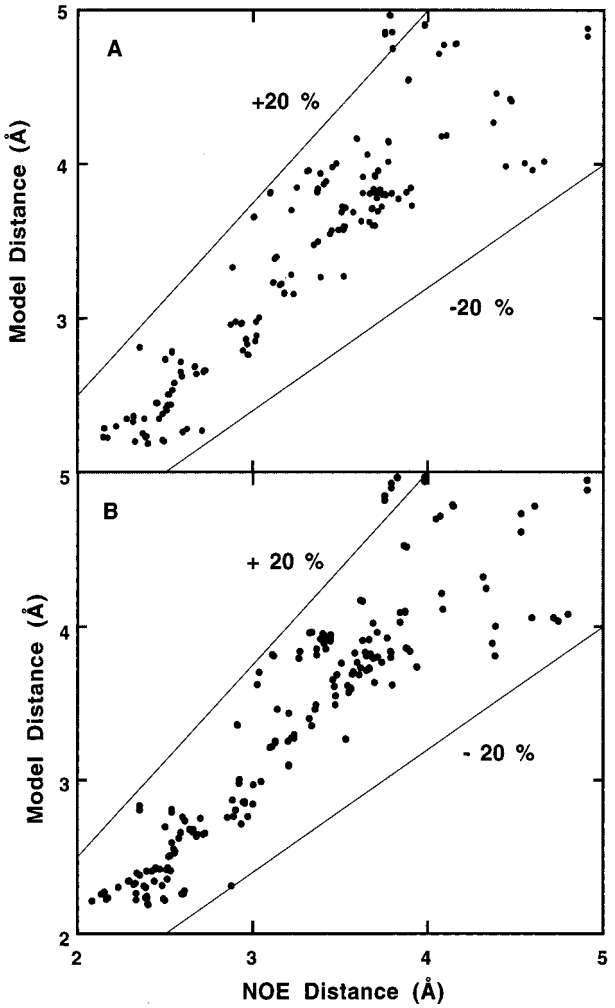

FIGURE 6: Correlation between the center of the experimental distance restraints and the actual distance from final structures of N3′ → P5′ phosphoramidate DNA isomer 1 (A) and isomer 2 (B).

with both calculated (*23*) and solid state (*22*) structures that the NP duplex is in a global A-form state. There are, however, very interesting and important differences among the three structures. There are also significant differences between the solution structure and the classical A-form conformation, and the similarities and differences for all of these helical duplexes will be presented below.

The structure determination protocols used in our work were designed to sample a wide range of conformational space to generate an ensemble of structures that is consistent with the NMR data and that incorporates spin diffusion effects by relaxation matrix calculations (IRMA). The possibility of starting structure dependency in the IRMA calculations was minimized by carrying out the refinement procedure on a range of initial structures obtained from both the A-form and B-form helical families and from randomized duplex structures generated by high-temperature SA. Only those distances were refined by the IRMA procedure that correspond to nonoverlapped NOE cross peaks. Other NOE distance and torsion angle constraints were incorporated into the restrained molecular dynamics and energy minimization calculations with larger boundaries appropriate for their experimental errors. The converged structures have low *R* values (Table 4), RMSDs, and constraint violations and excellent agreement between back-calculated and experimental NOESY spectra (Figures 6 and 7). All structure calculation protocols, whether starting from classical B- or A-helical families or from randomized helical structures from high-temperature SA, converged to the same limiting final ensemble of solution structures that are best visualized by the superimposed calculated structures shown in Figure 4A,B.

In our NMR analysis of the NP duplex in H_2O, we were unable to locate the NH protons of the phosphoramidate group that directly define isomers 1 and 2 (Figure 1). To obtain additional information about these protons, we collected spectra of the TnpT phosphoramidate-linked dinucleotide in D_2O, H_2O, and DMSO. The NH proton cannot be seen in either D_2O or H_2O but is observed as a broad peak in DMSO near room temperature, and the signal sharpens as the temperature is decreased (Figure 3). It is clear from these results, however, that the NH proton of NP exchanges with residual water in the DMSO very rapidly and exchanges much faster than the 5′-OH, 3′-OH, or imino protons. It is thus impossible to directly fix the orientation of the phosphoramidate group protons from NMR spectra in H_2O or D_2O, and we carried out the structure determination calculations with starting structures that are in both possible isomeric states of the NP group (Figure 1). For all of the methods that we have used, the global final structures calculated from isomer 1 and isomer 2 are quite similar, as can be seen by from the superimposed final structures in Figure 4C. The final structure from isomer 1 has lower energy and RMSD values than the final structure from isomer 2. The X-ray crystallographic analysis of the np(CGCGAATTCGCG)$_2$ duplex yielded structures for three very similar duplexes (*22*). H-bonds are observed between N−H groups and chloride ions in the crystal. These H-bonds specify the orientation of the phosphoramidate group as isomer 1 (Figure 1) in the crystal as in the low-energy solution conformation.

The final structures obtained from all refinement methods with NMR constraints are clearly in the global A-form helical conformation (Figures 5 and 7). A more quantitative analysis of the structure is provided by the backbone torsion angles in Table S1 and the plots of helical parameters in Figure 8. Backbone angles for both A- and B-helical structures have similar torsion angle values for α, β, γ, ϵ and ζ (*6*), and values in the expected range are found for all of these angles except those influenced by terminal effects (ϵ, ζ of C11, and α of G12 of strand 2 in the NP duplex, Table S1). The δ and χ angles for the A- and B-forms are significantly different, and all of the values for the NP duplex fall in the range expected for an A-form helix. It is clear from analysis of the NP duplex backbone structure that it falls into the A-form helix family.

A somewhat more complex picture of the structure is obtained from analysis of helical parameters (Figure 8). Base pairs in the B-helical conformation intersect the helix axis while, in the A-form, the base pairs are displaced into the minor groove, and the *x*-displacements for the NP duplex are into the minor groove as expected for an A-conformation. Although the displacement for the NP duplex never reaches as large a value as with the classical A-helix, it is very close to the A-form value. Comparison to displacements for crystal structures of the same sequence with phosphodiester (*30*) or phosphoramidate (*22*) backbones (Figure 8) clearly demonstrates the effect of the backbone modification with the diester values in the B-form range while the NP duplex

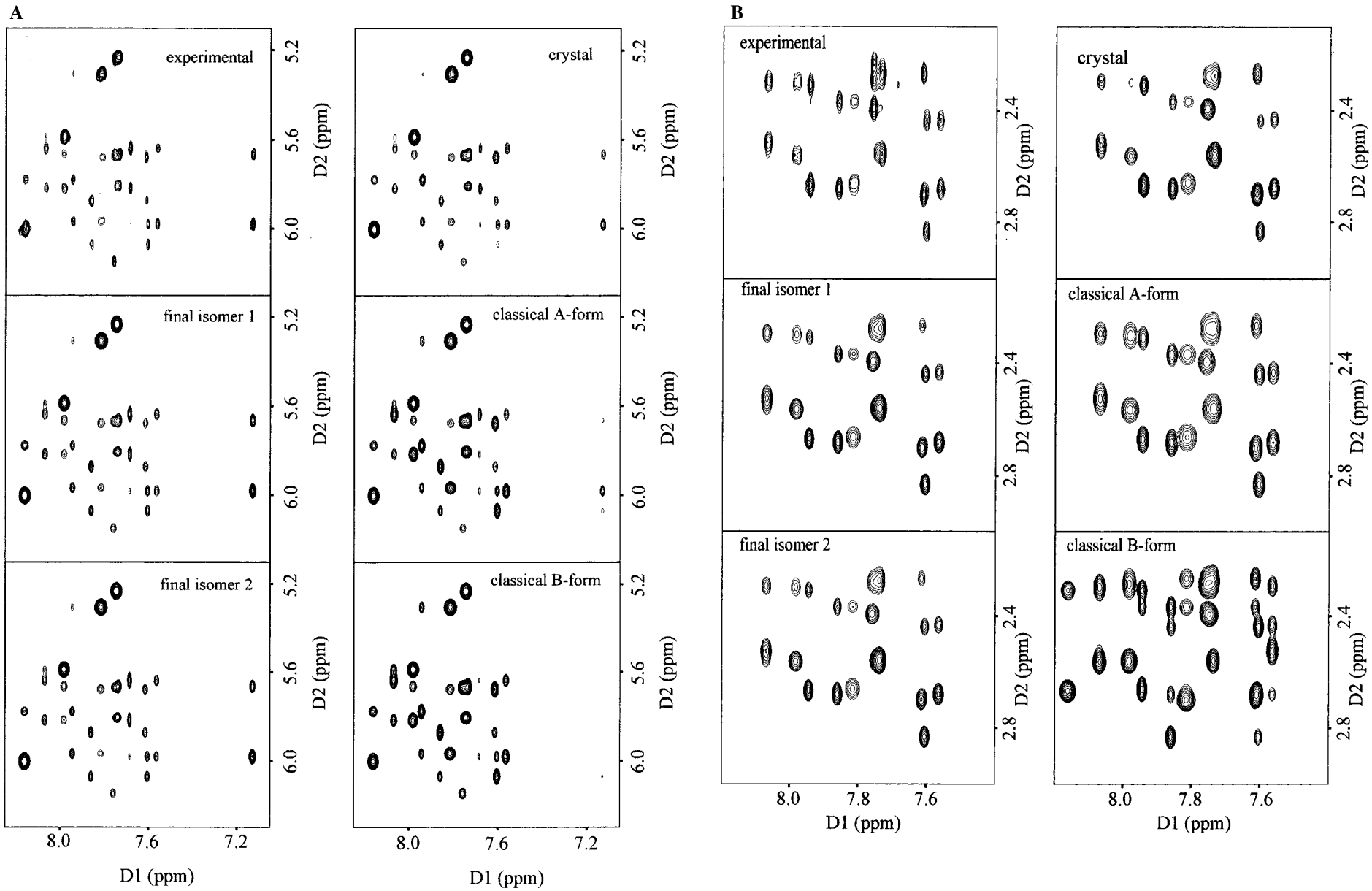

FIGURE 7: Experimental and back-calculated 300 ms NOESY spectra of the base H8/H6/H2 to H1′/H5 (A) and base to H2′/H2″ (B) regions for final structures for isomer 1 and isomer 2 as well as structures for the classical A-form and B-from and the NP crystal (*22*).

Table 4: *R*-Factors between the Experimental and Back-Calculated NOE Intensities for Classical Structures, Final Structures in the First and Second Refinement Protocols, and the Crystal Structure[a]

		R_1	R_2	R_7	R_8
classical	A-form	1.030	0.873	0.866	0.789
	B-form	0.667	0.630	0.829	0.790
first protocol final	A-isomer 1[b]	0.396	0.383	0.445	0.431
	B-isomer 1[b]	0.395	0.382	0.443	0.430
	A-isomer 2[b]	0.391	0.379	0.440	0.426
	B-isomer 2[b]	0.396	0.382	0.445	0.430
second protocol final	isomer 1	0.393	0.380	0.440	0.427
	isomer 2	0.390	0.378	0.440	0.426
crystal structure[c]		0.519	0.494	0.599	0.577

[a] See Materials and Methods for defination of R_1, R_2, R_7, and R_8. [b] A-isomer 1, B-isomer 1, A-isomer 2, and B-isomer 2 represent the final structures starting from A-form isomer 1, B-form isomer 1, A-form isomer 2, and B-form isomer 2, respecttively. [c] Ref *22*.

is more regular and in the A-form range. Base pair inclination is another important characteristic of the helix conformation with base pairs in the B-form close to perpendicular to the helix axis while those in the A-form are inclined approximately 20° (Figure 8). The inclination fluctuates along the NP duplex sequence but in general is less than for an A-helix but generally has values closer to those expected for an A-form rather than a B-form helix. Again, values from the crystal structures fall into the A-form range for the NP duplex with the diester structure having larger variations but falling closer to the B-form prediction. The base pair rise, which is also significantly different for the A- and B-helical forms, provides a similar illustration with the NP duplex values falling between the A-form and B-form values, but closer to the A-form values (Figure 8). The helical parameters for the diester structure have average values that are close to the B-form predictions, but the values have much larger variations than observed in the NP duplexes. The helical twist in Figure 8 provides another example of this trend in helical parameter differences and variation between the NP and diester duplexes.

Other important and very different characteristics of the A- and B-helical states are the major and minor groove widths which are extremely important for protein and small molecule recognition of nucleic acid duplexes. The major groove in the A-helix is much more narrow than in the B-form while the minor groove is wider than in the B-helix. As with other helical parameters described above, the groove widths of the NP duplex lie between the values for A- and B-structures but are closer to the A-form value. The conclusion from this analysis is that the NP duplex has backbone and sugar conformations that are very similar to those observed in classical A-helical structures while many of the helical parameters that characterize the global conformational state fall between those observed for A- and B-helical conformations. The final NP duplex structure is closer to the A-form conformation observed for some DNA sequences from X-ray studies than to the classical A-conformation of RNA. Egli and co-workers (*47*) have, for example, compared the crystal structures of the CCCCGGGG sequence as RNA and DNA A-type duplexes. Although both crystallize in the A-family, the RNA conforms closely to the classical prediction for an A-form helix, while the DNA has less inclination, a wider major groove, and other similar features and is closer to the conformation observed for the NP duplex in solution.

The X-ray structure is essentially identical to the solution structure in average values for the backbone angles and for base pair rise, slide, and twist. Relative to the NMR results, the solid state structure has a slightly larger *x*-displacement (4.2 versus 3.5 Å), larger inclination (14.7 vs 11.1 Å), and smaller major groove width (5.9 vs 7.0 Å); e.g., the X-ray structure is somewhat closer to the classical A-form than the NMR structure is. A back-calculated 2D NOESY spectrum from the coordinates of the X-ray structure is shown in Figure 7, and although the X-ray results do not produce as good a fit to the experimental solution data as the final NMR structure (the X-ray structure has an R_1 value of 0.51 while the value for the NMR structure is 0.39), they differ much less from the experimental results than do the classical A-form back-calculated spectra. Clearly, minor conformational changes occur in the solution conformation as it crystallizes. It is important to emphasize that although the solution and X-ray structures of the NP duplex were refined against different data sets, they are quite similar and are more regular than the phosphodiester of the same sequence (Figure 8). It appears that the NP backbone is preorganized into a very stable A-form type helical conformation that provides very strong interactions with other A-form helical nucleic acids and maintains very similar structures in both the solution and solid state.

The Kollman group has carried out unrestrained MD calculations on the dodecamer with phosphodiester and with N3′−P5′ linkages (*23*). The phosphodiester calculations included a term to incorporate the gauche effect between the O3′ and O4′ oxygens while the NP calculations did not have a similar gauche effect term. Under these conditions they obtain a B-form structure for the phosphodiester duplex and an A-form for the NP duplex. The predictions with respect to isomers 1 and 2 are less clear from the calculations. Calculations starting with the A-form yielded a mixture of both isomers. Calculations starting from the B-form in isomer 2 converted to an A-conformation while those starting with isomer 1 did not reach the A-form. There is very significant agreement between the global structures obtained by unrestrained MD and our structure obtained with NMR constrains. With the constraints in place, however, we find that isomer 1 (Figure 1) is the energetically favored configuration at the NP group. We do note fast exchange of the NH proton under standard solution conditions, however, and it is possible that in solution there is a population of isomer 2 in equilibrium with a more energetically favorable isomer 1 structure under normal conditions. The most important conclusion from both studies, however, is that a small change in electronegativity of the 3′ substituent can, through modification of the gauche effect, cause a shift in sugar conformational preference and, as a result, can cause major changes in global helix conformation.

An important question that arises from the structural analysis is why the deoxyribose duplex with NP linkages prefers an A-type conformation? NMR and X-ray studies on the sequence CGCGAA(T/U)(T/U)CGCG as DNA or RNA indicate that the DNA duplex has a B-type conformation while the isosequential RNA has an A-type duplex structure (*30*−*32*). The NMR solution structure presented here for the phosphoramidate duplex strongly supports our

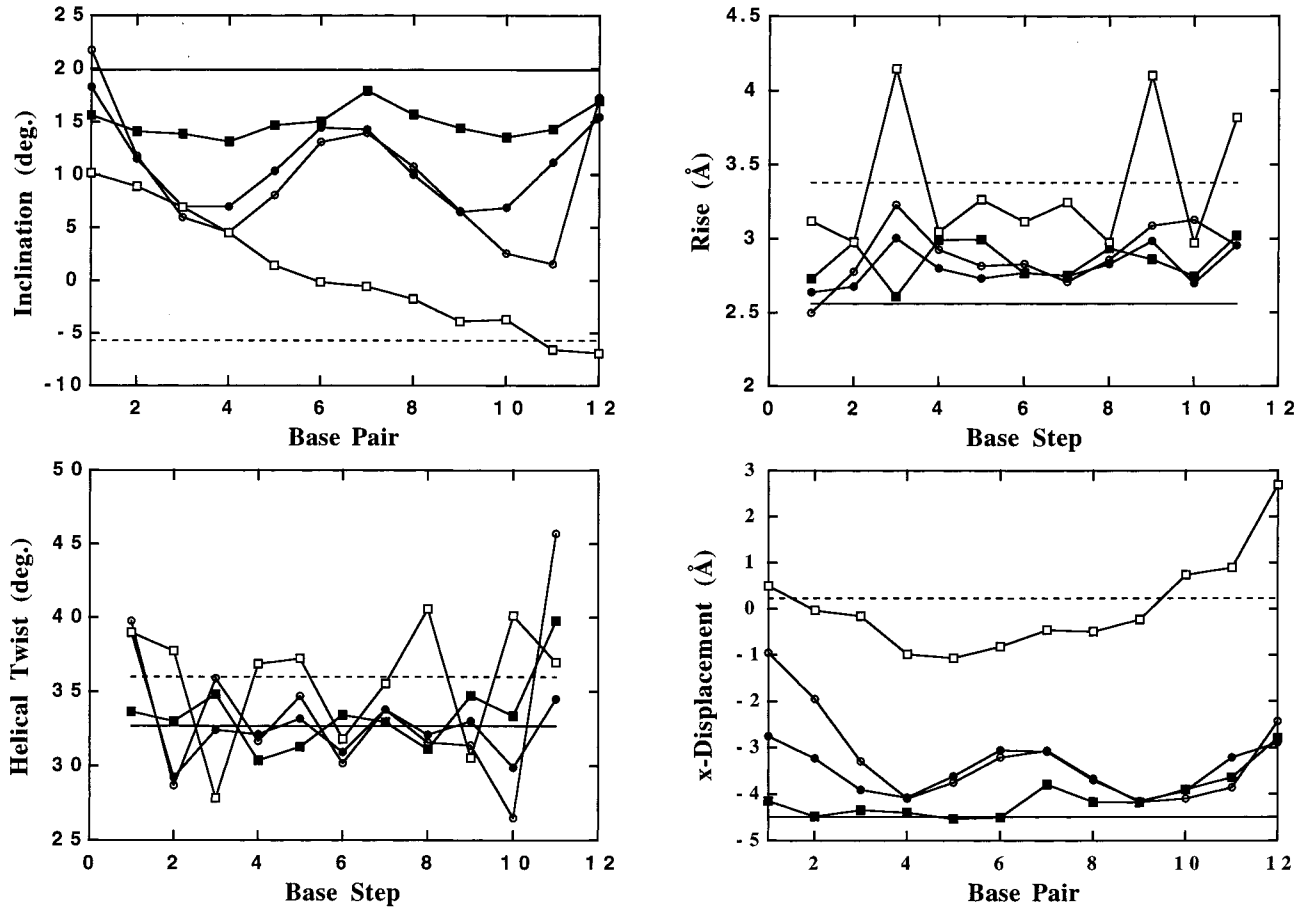

FIGURE 8: Graphical representation of helical parameters for the final structures for isomer 1 (●), isomer 2 (○), NP crystal structure (■) (*22*), and phosphodiester crystal structure (□) (*30*). Values expected from classical A-form (—) or B-form (- - -) helices are also indicated in the figures (calculated from the structures built with InsightII software).

earlier conclusions from CD and preliminary NMR studies, as well as modeling and X-ray crystallographic structures, which indicate that the NP duplex adopts an A-type helical structure both in solution and in the solid state. Ribose-type sugars with electronegative substituents at the 2′ position prefer the C3′-endo conformation range and lead to duplexes that generally prefer an A-form conformation (*6*). DNA with an H substituent at the 2′ position has been found in both the A- and B-helical conformations, but in solution the B-form conformation is observed under a wide range of conditions for most sequences (*6*). Chattopadhyaya and co-workers have conducted an extensive analysis of substituent effects at the 3′ position of 2′,3′-dideoxyribose and have found that with electronegative substituents the sugar prefers the S-conformational state but switches to an N-conformational preference as the electronegativity is decreased (*48*).

Our studies with the dinucleoside monophosphate d(TnpT) agree with the strong influence of the 3′-substituent and demonstrate that the 2′-deoxyribose substituted with a 3′-NP group is strongly biased to the N-conformational region by a combination of anomeric and gauche effects (*48*). These results indicate that substitution of the DNA phosphodiester by the N3′ → P5′ phosphoramidate linkage converts the nucleoside sugar pucker low-energy state from the S- to N-conformation even in single strands. This is the result expected from the interplay of gauche and anomeric substituent effects in the sugar ring system (*48*). It appears that the sugar conformational preference provides a small free energy drive that favors preorganization of each 3′-NH-substituted deoxyribose unit into a C3′-endo conformation and drives the backbone conformation of duplexes with this linkage into the A-form. In DNA with a normal phosphodiester linkage the sugars prefer the C2′-endo conformation under typical solution conditions, and this leads to a backbone preference for the B-form conformation. Other factors are clearly important in the final global conformation, however, and as described above, the NP duplex structure is closer to the conformation observed for some A-DNA sequences than to the classical A-conformation of RNA. The backbone of the NP duplex is apparently strongly dictated by the sugar conformation and is similar to the classical A-helix backbone. Without the influence of the 2′-OH group, however, some of the base pair conformational parameters fall between those for the A- and B-helical families (Figure 8) in both the solution and X-ray structures.

In conclusion, the backbone conformation of the NP duplex is apparently strongly dictated by the sugar conformation and is similar to the classical A-helix backbone. Without the influence of the 2′-OH group, however, some of the base pair conformational parameters fall between those for the A- and B-helical families (Figure 8) in both the solution and X-ray structures. Both solution and solid state analysis of the NP duplex conformation are in agreement that substitution of the 3′-O for 3′-NH results in an A-form helical structure with an isomer 1 configuration at the phosphoramidate NH groups. Although high-resolution

information is available only on the sequence CGCGAATTCGCG, CD spectra on other NP duplexes strongly suggest that DNAs with this backbone prefer the A-form conformation for a wide range of sequences (*17*, *21*). From both the conformational and molecular interaction (*21*) viewpoints, the conversion of the O−P−O to the N−P−O linkage produces DNA duplexes that behave much more like RNA than DNA.

ACKNOWLEDGMENT

We thank Professor Martin Egli, Northwestern University, for providing coordinates for the X-ray structure of the np-(CGCGAATTCGCG) duplex prior to publication and for very helpful discussions in this area. We also thank Professor Arther Pardi, University of Colorado, for providing the H-P Hetcor pulse sequence.

SUPPORTING INFORMATION AVAILABLE

One table providing backbone torsion angles, glycosidic torsion angles, and pseudorotation phase angles for individual nucleotides in the final isomer 1 and isomer 2 structures and three figures showing imino−imino and imino−aromatic regions of the 2D Watergate NOESY (Figure S1) of the NP duplex, general and selective $^{1}H-^{31}P$ HETCOR spectra of the NP duplex (Figure S2), and the H1′−H3′/H4′/H5′,H5″ cross-peak region of the 2D TOCSY with mixing times of 40 and 120 ms (Figure S3) of the duplex (4 pages). Ordering information is given on any current masthead page.

REFERENCES

1. Crooke, S. T., and Lebleu, B. (1993) *Antisense Research and Application*, CRC Press, Boca Raton, FL.
2. Sanghvi, Y. S., and Cook, P. D. (1994) in *Carbohydrate Modifications in Antisense Research* (Sanghvi, Y. S., and Cook, P. D., Eds.) pp 1−22, ACS Symposium Series, Washington, DC.
3. Miller, P. S. (1996) *Prog. Nucleic Acid Res. Mol. Biol. 52*, 261−291.
4. Agarwal, K. L., and Riftina, F. (1979) *Nucleic Acids Res. 6*, 3009−3024.
5. Crooke, S. T. (1997) *Ciba Found. Symp. 209*, 158−164.
6. Saenger, W. (1984) *Principles of Nucleic Acid Structure*, Springer, New York.
7. LaPlanche, L. A., James, T. L., Powell, C., Wilson, W. D., Uznanski, B., Stec, W. J., Summers, M. F., and Zon, G. (1986) *Nucleic Acids Res. 14*, 9081−9093.
8. Bower, M., Summers, M. F., Powell, C., Shinozuka, K., Regan, J. B., Zon, G., and Wilson, W. D. (1987) *Nucleic Acids Res. 12*, 4915−4931.
9. Cho, Y., Zhu, F. C., Luxon, B. A., and Gorenstein, D. G. (1993) *J. Biomol. Struct. Dyn. 11*, 685−702.
10. Jaroszewski, J. W., Clausen, V., Cohen, J. S., and Dahl, O. (1996) *Nucleic Acids Res. 24*, 829−834.
11. Mujeeb A., Reynolds, M. A., and James, T. L. (1997) *Biochemistry 36*, 2371−2379.
12. Bower, M., Summers, M. F., Powell, C., Shinozuka, K., Regen, J. B., Zon, G., and Wilson, W. D. (1987) *Nucleic Acids Res. 15*, 4915−4930.
13. Kibler-Herzog, L., Zon, G., Uznanski, B., Whitter, G., and Wilson, W. D. (1991) *Nucleic Acids Res. 19*, 2979−2986.
14. Kibler-Herzog, L., Zon, G., Whitter, G., Mizan, S., and Wilson, W. D. (1993) *Anti-Cancer Drug Des. 8*, 65−79.
15. Gryaznov, S. M., and Chen, J. K. (1994) *J. Am. Chem. Soc. 116*, 3143−3144.
16. Gryaznov, S. M., and Letsinger, R. L. (1992) *Nucleic Acids Res. 20*, 3403−3409.
17. Gryaznov, S. M., Lloyd, D. H., Chen, J. K., Schultz, R. G., DeDionisio, L. A., Ratmeyer, L., and Wilson, W. D. (1995) *Proc. Natl. Acad. Sci. U.S.A. 92*, 5798−5802.
18. Ding, D., Gryaznov, S. M., Lloyd, D. H., Chandrasekaran, S., Yao, S., Ratmeyer, L., Pan, Y., and Wilson, W. D. (1996) *Nucleic Acids Res. 24*, 354−360.
19. Zhou, S. B., Sun, J., Gryaznov, S. M., Liquier, J., Garestier, T., Helene, C., and Taillandier, E. (1997) *Nucleic Acids Res. 25*, 1782−1787.
20. Giovannangeli, C., Diviacco, S., Labrousse, V., Gryaznov, S., Charnau, P., and Helence, C. (1997) *Proc. Natl. Acad. Sci. U.S.A. 94*, 79−84.
21. Rigl, C. T., Lloyd, D. H., Tsou, D. S., Gryaznov, S. M., and Wilson, W. D. (1997) *Biochemistry 36*, 650−659.
22. Tereshko, V., Gryazonv, S., and Egli, M. (1998) *J. Am. Chem. Soc. 120*, 269−283.
23. Cieplak, P., Cheatham, T. E., and Kollman, P. A. (1997) *J. Am. Chem. Soc. 119*, 6722−6730.
24. Jones, K. A., and Peterlin, B. M. (1994) *Annu. Rev. Biochem. 63*, 717−743.
25. Karn, J., Gait, M. J., Churcher, M. J., Mann, D. A., Mikaelian, I., and Pritchard, C. (1994) in *RNA−Protein Interactions* (Nagai, K., and Mattaj, I. W., Eds.) pp 192−213, Oxford−IRL Press, Oxford.
26. Vaishnav, Y. N., and Wong-Staal, F. (1991) *Annu. Rev. Biochem. 60*, 577−630.
27. Cullen, B. R. (1995) *AIDS 9* (Suppl. A), S19−S32.
28. Gilboa, E., and Smith, C. (1994) *Trends Genet. 10*, 139−144.
29. Smith, C., Lee, S. W., Wong, E., Gallardo, H., Page, K., Gaspar, O., Lebowski, J., and Gilboa, E. (1996) *Antiviral Res. 32*, 99−115.
30. Dickerson, R. E., Drew, H. R., Conner, B. N., Wing, R. M., Fratin, A. V., and Kopka, M. L. (1982) *Science 216*, 475−485.
31. Lane, A. N., Jenkins, T. C., Brown, T., and Neidle, S. (1991) *Biochemistry 30*, 1372−1385.
32. Chou, S. H., Flynn, D., and Reid, B. R. (1989) *Biochemistry 28*, 2422−2435.
33. Hore, P. J. (1983) *J. Magn. Reson. 55*, 283−300.
34. Piotto, M., Saudek, V., and Sklenar, V. (1992) *J. Biomol. NMR 2*, 661−665.
35. Sklenar, V., Miyashiro, H., Zon, G., Miles, H. T., and Bax, A. (1986) *FEBS Lett. 208*, 94−98.
36. Sklenar, V., and Bax, A. (1987) *J. Am. Chem. Soc. 109*, 7525−7526.
37. Wuthrich, K. (1986) NMR of Proteins and Nucleic Acids, John Wiley and Sons, New York.
38. Veal, J. M., and Wilson, W. D. (1991) *J. Biomol. Struct. Dyn.*, 1119−1145.
39. Barsky, D., Colvin, M. E., Zon, G., and Gryaznov, S. M. (1997) *Nucleic Acids Res. 25*, 830−835.
40. Boelens, R., Koning, T. M. G., and Kaptein, R. (1988) *J. Mol. Struct. 173*, 229−311.
41. Wu, M., SantaLucia, J., Jr., and Turner, D. H. (1997) *Biochemistry 36*, 4449−4460.
42. Wang, H., Zuiderweg, E. R. P., and Glick, G. D. (1995) *J. Am. Chem. Soc. 117*, 2981−2991.
43. Zhu, L., and Reid, B. (1995) *J. Magn. Reson. B106*, 227−235.
44. Weiner, S. J., Kollman, P. A., Nguyen, D. T., and Case, D. A. (1986) *J. Comput. Chem. 7*, 230−252.
45. Wijmenga, S. S., Mooren, M. M. W., and Hilbers, C. W. (1993) in *NMR of Macromolecules, A Practical Approach* (Robertsm G. C. K., Ed.) pp 217−283, Oxford University Press, Oxford OX 2 6DP, U.K.
46. Schultze, P., and Feigon, J. (1997) *Nature 387*, 668.
47. Portmann, S., Usman, N., and Egli, M. (1995) *Biochemistry 34*, 7569.
48. Thibaudeau, C., Plavec, J., Garg, N., Papchikhin, A., and Chattopadhyaya, J. (1994) *J. Am. Chem. Soc. 116*, 4038−4043.

BI980711Y